arXiv:1601.07029v1 [nlin.PS] 24 Jan 2016

Stationary nonlinear waves, superposition modes and modulational instability characteristics in the AB system

Lei Wang[1,*], Zi-Qi Wang[2], Jian-Hui Zhang[2], Feng-Hua Qi[4], Min Li[1]

1. Department of Mathematics and Physics, North China Electric Power University, Beijing 102206, P. R. China

2. School of Energy Power and Mechanical Engneering, North China Electric Power University, Beijing 102206, P. R. China

3. School of Information, Beijing Wuzi University, Beijing 101149, P. R. China

[*]Corresponding author: 50901924@ncepu.edu.cn

Abstract

We study the AB system describing marginally unstable baroclinic wave packets in geophysical fluids and also ultra-short pulses in nonlinear optics. We show that the breather can be converted into different types of stationary nonlinear waves on constant backgrounds, including the multi-peak soliton, M-shaped soliton, W-shaped soliton and periodic wave. We also investigate the nonlinear interactions between these waves, which display some novel patterns due to the non-propagating characteristics of the solitons: (1) Two antidark solitons can produce a W-shaped soliton instead of a higher-order antidark one; (2) The interaction between an antidark soliton and a W-shaped soliton can not only generate a higher-order antidark soliton, but also form a W-shaped solion pair; (3) The interactions between an oscillation W-shaped soliton and an oscillation M-shaped soliton show the multi-peak structures. We find that the transition occurs at a modulational stability region in a low perturbation frequency region.

Solitons, breathers, and rogue waves have been observed widely in nonlinear optics and fluid mechanics. Recent studies have revealed the intricate relation between the soliton and breather (or rogue wave) solutions of certain higher-order and coupled nonlinear evolution equations. Breathers or rogue waves may be converted into various nonlinear waves on constant backgrounds. The interactions among these transformed waves show some novel characteristics. Hereby, we will consider the AB system describing marginally unstable baroclinic wave packets in geophysical fluids and also ultra-short pulses in nonlinear optics. Several types of transformed stationary nonlinear waves will be demonstrated under some special conditions. Due to the non-propagating characteristic, the nonlinear superpositions include some interesting phenomena. Further, the transformed nonlinear waves are associated with a modulational stability region in a low perturbation frequency region.

1. Introduction

Echoing soliton concepts that flourished in the multidisciplinary since a few decades ago, rogue wave has attracted recently the attention of researchers in various physical settings, e.g., in hydrodynamics [1], capillary waves [2], plasma physics [3], nonlinear optics [4], and Bose-Einstein condensation [5]. Due to their harm to various hydrotechnic constructions, the investigation of rogue waves becomes a very important problem [6]. Rogue waves, which have a peak amplitude generally more than twice the significant wave height, are thought to appear from nowhere and disappear without a trace in the ocean and most experimental optical systems [7]. Among various models describing such waves, the focusing nonlinear Schrödinger (NLS) equation [8] is the most accepted one. The NLS equation admits a type of rational solution that is localized in both space and time, i.e., the Peregine soliton [9]. This simplest rational solution of the NLS equation, which was first predicted as far as 30 years ago [9], is frequently used as a model of a rogue wave [10]. Breather solutions are presently regarded as potential prototypes for the rogue waves in many fields of physics [11]. Breathers develop due to the instability of small amplitude perturbations that may grow in size to disastrous proportions [12]. There are two types of breathers, namely, the Kuznetsov-Ma breathers (KMBs) [13] and Akhmediev breathers (ABs) [14]. The KMBs are periodic in space and localized in time while the ABs are periodic in time and localized in space [13, 14]. Taking the period of both solutions to infinity leads to a first-order doubly localized Peregrine soliton.

The modulational instability (MI) is generally considered to be one of factors which may give rise to rogue-wave excitation [9]. As a fundamental characteristic of many nonlinear dispersive systems, MI is related to the growth of periodic perturbations on an unstable continuous-wave background [15]. A rogue wave may be the result of MI, but not every type of MI results in rogue wave generation [16]. One of theoretical researches has revealed the close relationship between rogue waves and baseband MI, i.e., MI whose bandwidth includes components of arbitrarily low frequency [17, 18]. Another possible explanation presented by Zhao and Ling is that rogue wave comes from MI under the "resonance" perturbation with continuous wave background [19].

Recent studies have revealed the intricate link between the rogue waves (or breathers) and solitons of a certain class of nonlinear evolution equations. When the eigenvalues meet a certain locus on the complex plane, Akhmediev *et al.* have discovered that the breather solutions of the Hirota [20] equation and fifth-order NLS [21] equation can be converted into soliton solutions on a background, which does not exist in the standard NLS equation. He *et al.* have reported that the rational solution of a mixed NLS equation can describe five soliton states, including a paired bright-bright soliton, a single soliton, a paired bright-grey soliton, a paired bright-black soliton, and a rogue wave state [22]. They have found that the state transition among these five states is induced by tuning the effects of self-steepening and self-phase modulation. Liu *et al.* have shown that the breathers can be converted into different types of nonlinear waves in the coupled NLS-MB system, including the multipeak soliton, periodic wave, antidark soliton, and

W-shaped soliton [23]. In particular, they have indicated that the transition between the rogue waves and W-shaped solitons of the Hirota and coupled Hirota equations occurs as a result of the attenuation of MI growth rate to vanishing in the zero-frequency perturbation region [24].

In this paper, we study the AB system [25, 26],

$$\begin{aligned}&(\frac{\partial}{\partial T}+c_1\,\frac{\partial}{\partial X})(\frac{\partial}{\partial T}+c_2\,\frac{\partial}{\partial X})\,A=l_1\,A-l_2\,A\,B,\\&(\frac{\partial}{\partial T}+c_2\,\frac{\partial}{\partial X})\,B=(\frac{\partial}{\partial T}+c_1\,\frac{\partial}{\partial X})|A|^2\,,\end{aligned}\tag{1}$$

where A is the amplitude of the wave packet and B is a quantity measuring the correction of the basic flow due to the wave packet, T and X denote the time and space variables, respectively, c_1 and c_2 stand for two group velocities of the underlying linear problem, and l_1 represents a parameter measuring the state of the basic flow. When the basic flow is super-critical, $l_1>0$, and when the basic flow is sub-critical, $l_1<0$. The parameter l_2 reflects the interaction of the wave packet and the meanflow, and it is always positive. System (1) describes marginally unstable baroclinic wave packets in geophysical fluids and also ultra-short pulses in nonlinear optics.

As shown in Ref. [27], System (1) can be reduced to a simpler form

$$A_{xt}=\alpha\,A+\beta\,A\,B,\quad B_x=-\frac{1}{2}\gamma(|A|^2)_t\,,\tag{2}$$

with

$$\alpha=\frac{n_1\,c_2}{(c_1-c_2)^2}\,,\quad \beta=-\frac{n_2\,c_2}{(c_1-c_2)^2}\,,\quad \gamma=-\frac{2}{c_2}\,,\tag{3}$$

by the transformations

$$x=X-c_1\,T,\quad t=T-\frac{X}{c_2}\,.\tag{4}$$

Recently, certain properties of System (2) have been investigated. System (2) can be transformed to the Sine-Gordon equation when A is the real value and to the self-induced transparency system when A is the complex value [25, 26]. Lax pair and some periodic solutions of System (2) have been derived in Ref. [26]. MI and breather dynamics of System (2) have been discussed in Ref. [28]. Ref. [29] has studied the envelope solitary waves and periodic waves of System (2). The higher-order rogue wave solutions of System (2) have been found via the modified Darboux transformation (mDT) in Ref. [30]. The semirational solutions have been derived in Ref. [18] and the link between the baseband MI and the existence condition of these rogue waves has been revealed. Recently, the rogue waves and MI have been demonstrated for a coupled AB system, i.e., a wave-current interaction model describing baroclinic instability processes in geophysical flows [27].

The aim of the present paper is to study the breather-soliton dynamics of System (2). We present intriguing different kinds of nonlinear localized and periodic waves, including the

multi-peak soliton, M-shaped soliton, W-shaped soliton and periodic wave. Interestingly, these waves are stationary nonlinear waves with respect to x-axis. Further, due to the nonpropagating characteristic, the nonlinear interactions show some novel properties. The breather-to-soliton transition is related to a special type of MI analysis that involves a MI stability region in a low perturbation frequency region.

The arrangement of the paper is as follows: In Sec. 2, we will present different types of stationary nonlinear waves of System (2), including the multi-peak soliton, M-shaped soliton, W-shaped soliton and periodic waves. And the transition condition will be analytically given. The properties of interactions between different types of nonlinear waves will be graphically studied in Sec. 3. The connection between the MI growth rate and transition condition will be revealed in Sec. 4. Finally, Sec. 5 will be the conclusions of this paper.

2. Different types of stationary nonlinear waves

In this section, we mainly study the transitions between the first-order breather and various nonlinear waves for System (2). The first-order breather solution of System (2) is given [18]

$$\begin{aligned} A_B^{[1]} &= \left(a + n_1 \frac{G_B^{[1]} + i\, H_B^{[1]}}{D_B^{[1]}}\right) e^{i\,\rho}\,, \\ B_B^{[1]} &= b + \frac{4\,i}{\beta}\left(\frac{m_1\, E_B^{[1]} + i\, n_1\, F_B^{[1]}}{D_B^{[1]}}\right)_t, \end{aligned} \tag{5}$$

with

$$\begin{aligned} &\rho = \omega\, x + k\, t\,, \qquad k = -\frac{\alpha + b\,\beta}{\omega}\,, \\ &G_B^{[1]} = k_1\, k_2\, \cos(t\, V_H + x\, h_R)\cosh(2\,\chi_I) - \cosh(t\, V_T + x\, h_I)\sin(2\,\chi_R)\,, \\ &H_B^{[1]} = k_1\, k_2\, \sin(t\, V_H + x\, h_R)\sinh(2\,\chi_I) + \cos(2\,\chi_R)\sinh(t\, V_T + x\, h_I)\,, \\ &D_B^{[1]} = -k_1\, k_2\, \cos(t\, V_H + x\, h_R)\sin(2\,\chi_R) + \cosh(t\, V_T + x\, h_I)\cosh(2\,\chi_I)\,, \\ &E_B^{[1]} = k_1\, k_2\, \cos(t\, V_H + x\, h_R)\sin(2\,\chi_R) - \cosh(t\, V_T + x\, h_I)\cosh(2\,\chi_I)\,, \\ &F_B^{[1]} = k_1\, k_2\, \sin(t\, V_H + x\, h_R)\cos(2\,\chi_R) - \sinh(t\, V_T + x\, h_I)\sinh(2\,\chi_I)\,, \\ &h = \sqrt{a^2\beta\gamma + (2\,\lambda + \omega)^2} = h_R + i\, h_I\,, \\ &\chi = \frac{1}{2}\,\arccos(\frac{h}{2})\,, \quad \varpi = \frac{h}{2}\left(x + \frac{k}{2\,\lambda}\,t\right) = (x + (\varpi_R + i\,\varpi_I)t)\frac{h}{2}\,, \\ &V_T = 2(\varpi_R\, h_I + \varpi_I\, h_R)\,, \qquad V_H = 2(\varpi_R\, h_R - \varpi_I\, h_I)\,, \\ &k_1 = 1,\, k_2 = \pm 1\,. \end{aligned}$$

From the above expression, one can find that the breather solution (5) comprises the hyperbolic functions $\sinh F$ ($\cosh F$) and the trigonometric functions $\sin G$ ($\cos G$), where $\varpi_R + \frac{\varpi_I h_R}{h_I}$ and $\varpi_R - \frac{\varpi_I h_I}{h_R}$ are the corresponding velocities. The hyperbolic functions and trigonometric functions, respectively, characterize the localization and the periodicity of the transverse distribution t of

those waves. The nonlinear wave described by the solution (5) can be deemed to a nonlinear combination of a soliton and a periodic wave with the velocities $\varpi_R + \frac{\varpi_I h_R}{h_I}$ and $\varpi_R - \frac{\varpi_I h_I}{h_R}$. In the following, we show that the solution (5) can describe different kinds of nonlinear wave states depending on the values of velocity difference $\frac{\varpi_I(h_R^2+h_I^2)}{h_R h_I}$.

When $\varpi_I(\frac{h_R^2+h_I^2}{h_R h_I}) \neq 0$ (or $\varpi_I \neq 0$), the solution (5) characterizes the localized waves with breathing behavior on constant backgrounds (i.e., the breathers and rogue waves). Further, if $m = -\frac{\omega}{2}$, we have the ABs with $|n| < |\frac{a\sqrt{\beta\gamma}}{2}|$, the KMBs with $|n| > |\frac{a\sqrt{\beta\gamma}}{2}|$, and the Peregrine soliton with $|n| = |\frac{a\sqrt{\beta\gamma}}{2}|$. Those solutions have been obtained in Refs. [18, 28, 30].

Conversely, if $\varpi_I = 0$, the soliton and a periodic wave in the solution (5) have the same velocity ϖ_R. Meanwhile, we should point out that the case $\varpi_I = 0$ is equivalent to the following condition

$$\frac{V_T}{h_I} = \frac{V_H}{h_R}\,, \tag{6}$$

i.e.,

$$b = -\frac{\alpha}{\beta}\,. \tag{7}$$

Eq. (6) means the extrema of trigonometric and hyperbolic functions in the solution (5) is located along the same straight lines in the (x,t)-plane, which results in the transformation of the breather into a continuous soliton. Additionally, the case $b = -\frac{\alpha}{\beta}$ is also equivalent to $k = 0$. Then, the parameters ϖ_R, ϖ_I, V_T and V_H vanish, and the solution (5) only depends on x and is independent of t. Thus, the nonlinear waves described by the solution (5) possess the nonpropagating characteristic.

Under the transition condition (7), we demonstrate several kinds of transformed nonlinear waves on constant background for A, including the multi-peak solitons, M-shaped soliton, periodic waves and W-shaped soliton. We omit the results in the B component, since it only describes the plane wave in the case of $k = 0$. **Fig. 1** shows a multi-peak soliton on constant background that does not propagate along x direction. Such structure is composed of a soliton and periodic wave. Adding the absolute value of real part to the eigenvalue, $|m|$, we find that the peak numbers of multi-peak localized structure decrease, as depicted in **Fig. 2**. From the cross-sectional views, it is observed that both of those multi-peak solitons have one main peak which is located at $(0,0)$. The maximum amplitude of $|A|^2$ at $(0,0)$ can be given analytically

$$|A(0,0)|^2 = (a - 4\,\frac{n}{\sqrt{\beta\gamma}})^2\,. \tag{8}$$

Eq. (8) indicates that the imaginary part of eigenvalue (n) has real effects on the maximum amplitude of $|A|^2$ at $(0,0)$.

Further, the structure in Fig. 2 (we call it an oscillation W-shaped soliton) corresponds to the case $|A(0,0)|^2_{xx} > 0$ with the appropriate value of n ($n = -0.7$). In other words, the

coordinate origin $(0,0)$ is a local maximum of $|A(x,0)|^2$. Nevertheless, when the value of n exceeds a certain range, $|A(0,0)|^2_{xx}$ is less than zero, which means that the coordinate origin $(0,0)$ is a local minimum of $|A(x,0)|^2$. In this case, the oscillation W-shaped soliton translates into a M-shaped soliton shown in **Fig. 3**. It is observed that this structure has two main peaks with identical amplitudes. In order to reveal the effect of the value of n on $|A(0,0)|^2_{xx}$, we plot **Fig. 4** with $a = 2$, $b = 1$, $\gamma = 1$, $\omega = 1$, $\alpha = -1$, $\beta = 1$, $k_1 = 1$, $k_2 = -1$ and $m = -0.8$. If $0 < n < 1.25$, namely, $|A(0,0)|^2_{xx} < 0$, the solution (5) describes the M-shaped soliton whereas it describes the W-shaped one.

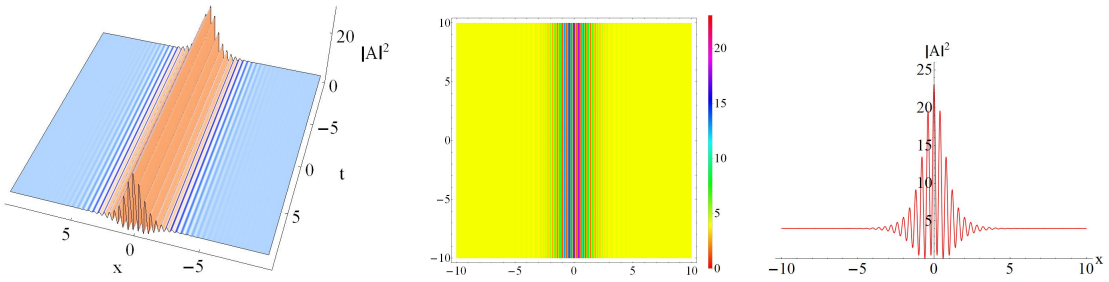

(a) (b) (c)

Figure 1: A breather transformed into a multi-peak soliton with $a = 2$, $b = 1$, $\gamma = 1$, $\omega = 1$, $\alpha = -1$, $\beta = 1$, $k_1 = 1$, $k_2 = -1$ and $\lambda_1 = \lambda_2^* = 7.2 - 0.7\,i$. (b) is the contour plot of (a). (c) is the cross-sectional view of (a) at $t = 0$.

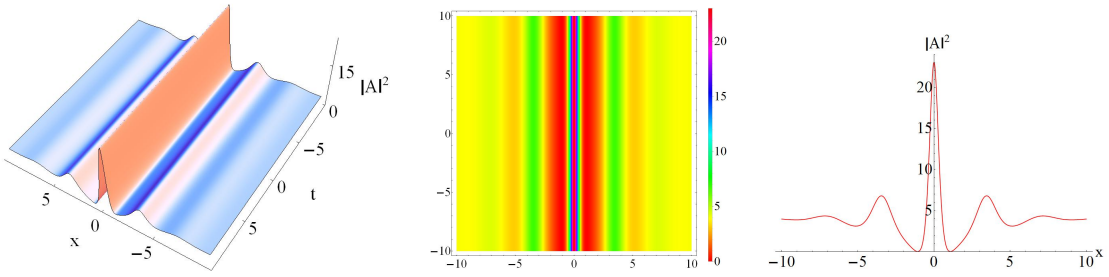

(a) (b) (c)

Figure 2: A breather transformed into an oscillation W-shaped soliton with $a = 2$, $b = 1$, $\gamma = 1$, $\omega = 1$, $\alpha = -1$, $\beta = 1$, $k_1 = 1$, $k_2 = -1$ and $\lambda_1 = \lambda_2^* = -0.8 - 0.7\,i$. (b) is the contour plot of (a). (c) is the cross-sectional view of (a) at $t = 0$.

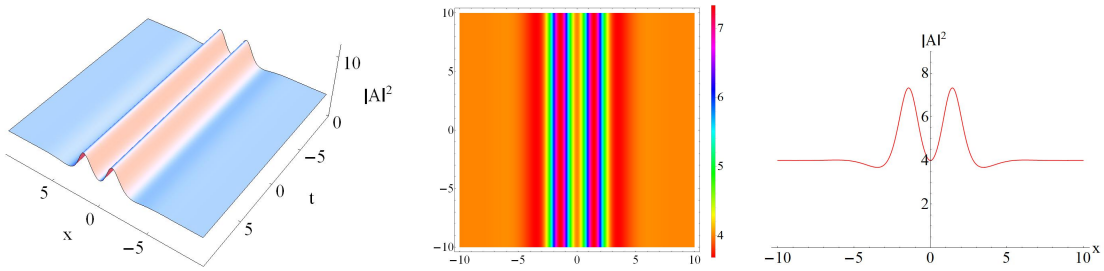

(a) (b) (c)

Figure 3: A breather transformed into a M-shaped soliton with $a = 2$, $b = 1$, $\gamma = 1$, $\omega = 1$, $\alpha = -1$, $\beta = 1$, $k_1 = 1$, $k_2 = -1$ and $\lambda_1 = \lambda_2^* = -0.8 + i$. (b) is the contour plot of (a). (c) is the cross-sectional view of (a) at $t = 0$.

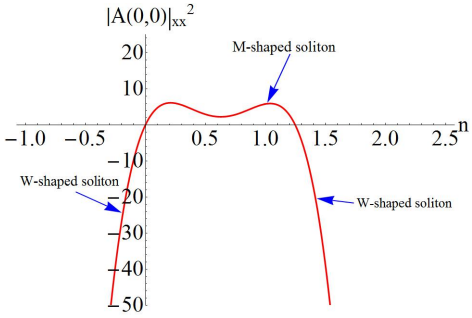

Figure 4: Effects of the imaginary part of eigenvalue n on $|A(0,0)|_{xx}^2$ with $a = 2$, $b = 1$, $\gamma = 1$, $\omega = 1$, $\alpha = -1$, $\beta = 1$, $k_1 = 1$, $k_2 = -1$ and $m = -0.8$. Two zeros of the $|A(0,0)|_{xx}^2$ are in $(0,0)$ and $(1.25,0)$ respectively.

Next, we derive two special nonlinear waves from the solution (5), i.e., the antidark soliton and periodic wave. The former exists in isolation when h_R vanishes, while the latter independently exists when h_I vanishes. Therefore, the antidark soliton and periodic wave are shown in forms of exponential and trigonometric functions respectively. Specifically, the analytical expressions read as, for the soliton,

$$A_S^{[1]} = (a + n_1 \frac{G_S^{[1]} + i\, H_S^{[1]}}{D_S^{[1]}})\, e^{i\,\rho}\,, \quad B_S^{[1]} = b\,, \tag{9}$$

with

$$\begin{aligned} G_S^{[1]} &= k_1\, k_2\, \cosh(2\,\chi_I) - \cosh(x\, h_I)\sin(2\,\chi_R)\,, \\ H_S^{[1]} &= \cos(2\,\chi_R)\sinh(x\, h_I), \\ D_S^{[1]} &= -k_1\, k_2\, \sin(2\,\chi_R) + \cosh(x\, h_I)\cosh(2\,\chi_I)\,, \end{aligned} \tag{10}$$

and for the periodic wave,

$$A_P^{[1]} = (a + n_1 \frac{G_P^{[1]} + i\, H_P^{[1]}}{D_P^{[1]}})\, e^{i\,\rho}\,, \quad B_P^{[1]} = b\,. \tag{11}$$

with

$$
\begin{aligned}
G_P^{[1]} &= k_1\, k_2\, \cos(x\, h_R)\cosh(2\,\chi_I) - \sin(2\,\chi_R)\,, \\
H_P^{[1]} &= k_1\, k_2\, \sin(x\, h_R)\sinh(2\,\chi_I)\,, \\
D_P^{[1]} &= -k_1\, k_2\, \cos(x\, h_R)\sin(2\,\chi_R) + \cosh(2\,\chi_I)\,.
\end{aligned}
\tag{12}
$$

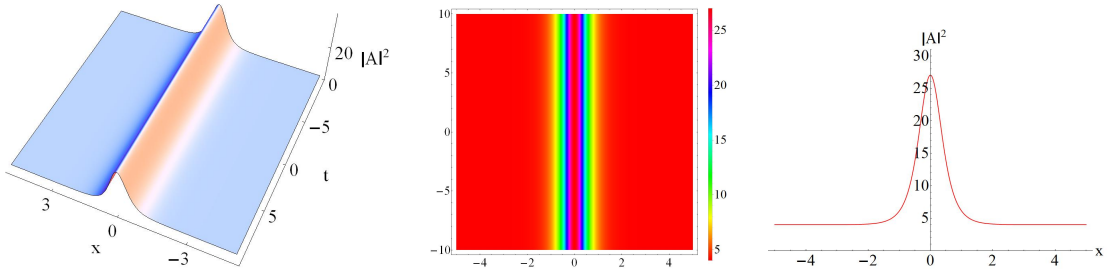

Figure 5: A breather transformed into an antidark soliton with $a = 2$, $b = 1$, $\gamma = 1$, $\omega = 1$, $\alpha = -1$, $\beta = 1$, $k_1 = 1$, $k_2 = 1$ and $\lambda_1 = \lambda_2^* = -0.5 - 1.8\,i$. (b) is the contour plot of (a). (c) is the cross-sectional view of (a) at $t = 0$.

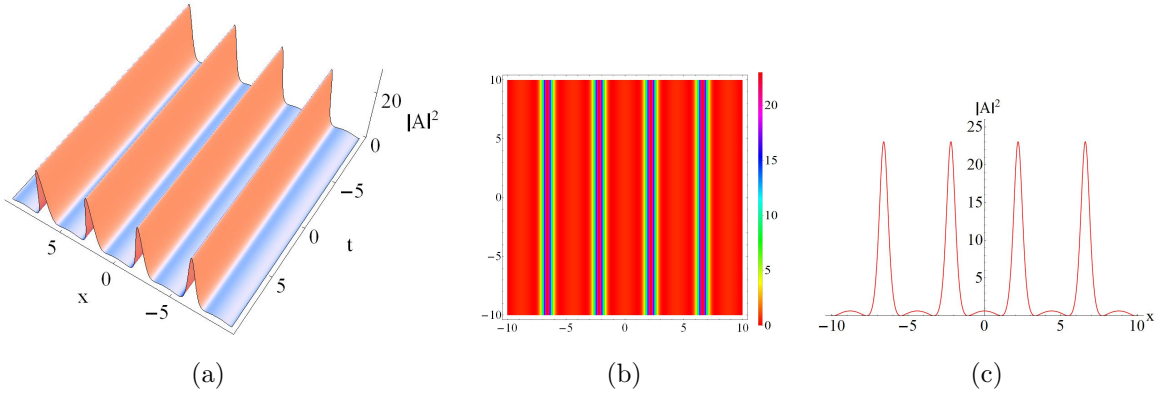

Figure 6: A breather transformed into a periodic wave with $a = 2$, $b = 1$, $\gamma = 1$, $\omega = 1$, $\alpha = -1$, $\beta = 1$, $k_1 = 1$, $k_2 = -1$ and $\lambda_1 = \lambda_2^* = -0.5 + 0.7\,i$. (b) is the contour plot of (a). (c) is the cross-sectional view of (a) at $t = 0$.

Fig. 5 describes a soliton that does not propagate along x direction. It is shown that this soliton lies on a plane-wave background with the peak $(a\sqrt{\beta\gamma} - 2\,n)^2$. This kind of wave is referred to the antidark soliton which was firstly reported in the scalar NLS system with the third-order dispersion [31]. Recent studies on the NLS-MB system have also presented the similar structures [23]. Further, for the value of a becomes zero, this soliton will be converted into a standard bright soliton. **Fig. 6** exhibits the periodic wave with the period $P = \frac{\pi}{h_R}$. It is interesting, as it looks like higher-order wave but appears from the same solution.

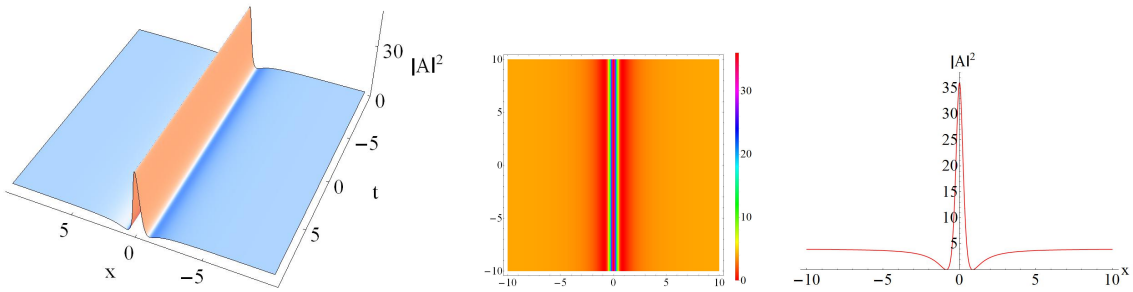

(a) (b) (c)

Figure 7: A rogue wave transformed into a W-shaped soliton with $a = 2$, $b = 1$, $\gamma = 1$, $\omega = 1$, $\alpha = -1$, $\beta = 1$, $k_1 = 1$, $k_2 = 1$ and $\lambda_1 = \lambda_2^* = -0.5 + i$. (b) is the contour plot of (a). (c) is the cross-sectional view of (a) at $t = 0$.

In particular, as the period h_R is close to zero, namely, $n \to a\sqrt{\beta\gamma}$, the periodic wave will turn into the W-shaped soliton, as shown in **Fig. 7**. In this case, the solution (5) is transformed into

$$A_{RS}^{[1]} = -\frac{a\, e^{ix\omega}\,(a^2\,\beta\,\gamma\,x^2 - 3)}{a^2\,\beta\,\gamma\,x^2 + 1}\,. \tag{13}$$

The maximum height ($9a^2$) of the W-shaped wave is nine times the background intensity while the minimum is zero. By comparison with the W-shaped soliton in Fig. 2, the soliton in Fig. 7 has two different features: (1) it shows a single-peak structure without oscillating tails; (2) it has a rational expression.

We further discuss the effects of the coefficients α, β and γ on the transformed solitons. The coefficients α, β and γ, which are related to the parameters c_1, c_2, l_1 and l_2, are defined by the equation (3). **Figs. (8a)** and **(8b)** indicate that the amplitudes of the multi-peak solitons decrease with increasing the values of β and γ. In addition, increasing the values of β and γ leads to stronger localization and a smaller oscillation period for the multi-peak soliton. This means that we can control the amplitudes of the transformed nonlinear waves by adjusting the two group velocity coefficients c_1 and c_2, and the parameter l_2 that reflects the interaction of the wave packet and the meanflow. However, as shown in **Fig. (8c)**, changing the value of α doesn't affect the characteristics of the multi-peak soliton.

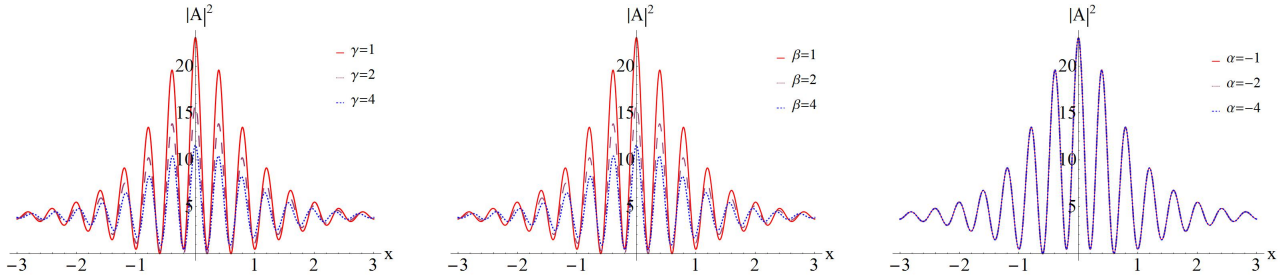

(a) (b) (c)

Figure 8: The effects of α, β and γ on the multi-peak solitons with $a = 2, \omega = 1, k_1 = 1, k_2 = -1$ and $\lambda_1 = \lambda_2^* = 7.2 - 0.7\,i$. $(a) : \alpha = -1, \beta = 1; (b) : \alpha = -1, \gamma = 1; (c) : \beta = 1, \gamma = 1$.

3. Nonlinear wave interactions

In this section, we study the characteristics of interactions between the nonlinear waves presented above. Due to the diversity of the transformed waves (in fact, there are many kinds of nonlinear wave interactions), we only exhibit several typical nonlinear superposition patterns that derive from the two-breather solutions.

By virtue of the n-fold DT [18, 28], the two-breather solution of System (2) is given as

$$A_B^{[2]} = A^{[0]} + \frac{4\,i}{\sqrt{\beta\gamma}}\frac{\Delta_1^{[2]}}{\Delta^{[2]}}, \qquad B_B^{[2]} = B^{[0]} - \frac{4\,i}{\beta}\left(\frac{\Delta_2^{[2]}}{\Delta^{[2]}}\right)_t, \tag{14}$$

with

$$\begin{aligned}
&A^{[0]} = a\,e^{i\,\rho}, \quad B^{[0]} = b,\\
&\lambda_1 = \lambda_2^* = m_1 + n_1\,i, \quad \lambda_3 = \lambda_4^* = m_2 + n_2\,i,\\
&\psi_2 = -\varphi_1^*, \quad \varphi_2 = \psi_1^*; \quad \psi_4 = -\varphi_3^*, \quad \varphi_4 = \psi_3^*;\\
&\varphi_j = k_1\frac{i\,h_j + 2\,i\,\lambda_j + i\,\omega}{a\sqrt{\beta\gamma}}\,e^{i\,(\varpi_j + \frac{\rho}{2})} + k_2\,e^{-i(\varpi_j - \frac{\rho}{2})},\\
&\psi_j = k_1\,e^{i\,(\varpi_j - \frac{\rho}{2})} + k_2\frac{i\,h_j + 2\,i\,\lambda_j + i\,\omega}{a\sqrt{\beta\gamma}}\,e^{-i(\varpi_j + \frac{\rho}{2})},\\
&j = 1, 3, \quad k_1 = k_2 = 1,\\
&\Delta_1^{[2]} = \begin{vmatrix} \lambda_1\varphi_1 & \varphi_1 & -\lambda_1^2\varphi_1 & \psi_1\\ \lambda_2\varphi_2 & \varphi_2 & -\lambda_2^2\varphi_2 & \psi_2\\ \lambda_3\varphi_3 & \varphi_3 & -\lambda_3^2\varphi_3 & \psi_3\\ \lambda_4\varphi_4 & \varphi_4 & -\lambda_4^2\varphi_4 & \psi_4 \end{vmatrix}, \quad \Delta_2^{[2]} = \begin{vmatrix} -\lambda_1^2\varphi_1 & \varphi_1 & \lambda_1\psi_1 & \psi_1\\ -\lambda_2^2\varphi_2 & \varphi_2 & \lambda_2\psi_2 & \psi_2\\ -\lambda_3^2\varphi_3 & \varphi_3 & \lambda_3\psi_3 & \psi_3\\ -\lambda_4^2\varphi_4 & \varphi_4 & \lambda_4\psi_4 & \psi_4 \end{vmatrix},\\
&\Delta^{[2]} = \begin{vmatrix} \lambda_1\varphi_1 & \varphi_1 & \lambda_1\psi_1 & \psi_1\\ \lambda_2\varphi_2 & \varphi_2 & \lambda_2\psi_2 & \psi_2\\ \lambda_3\varphi_3 & \varphi_3 & \lambda_3\psi_3 & \psi_3\\ \lambda_4\varphi_4 & \varphi_4 & \lambda_4\psi_4 & \psi_4 \end{vmatrix}.
\end{aligned}$$

Fig. 9 displays the elastic interaction between two breathers of System (2). It is found that the two-breather interaction produces a second-order central rogue wave in (x-t) plane. Similar to the case in Section 2, to convert the two-breather solutions into the two-soliton ones on constant backgrounds, the parameter b also needs to meet the transition condition (7), namely, $k = 0$. For different kinds of nonlinear superpositions, we can choose the corresponding real (m_j) and imaginary (n_j) parts of eigenvalues (λ_j) in the solution (14). The values of m_j and n_j ($j = 1, 3$) control the types of the transformed nonlinear waves. In the following, we present six kinds of nonlinear superposition patterns.

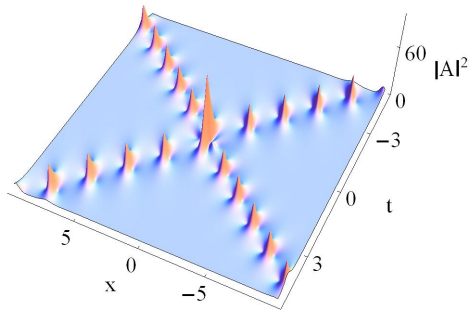

Figure 9: Elastic collision between two breathers with $a = 2$, $b = 1$, $\gamma = 4$, $\omega = 1$, $\alpha = 4$, $\beta = 1$, $k_1 = 1$, $k_2 = 1$, $\lambda_1 = \lambda_2^* = 1.8\,i$ and $\lambda_3 = \lambda_4^* = -0.8 + 1.8\,i$.

The oscillation W-shaped soliton. We first consider the nonlinear superposition of two stationary W-shaped solitons, which is exhibited in **Fig. 10**. The two eigenvalues $\lambda_1 = -0.5{+}2.1\,i$ and $\lambda_3 = -0.5 + 2.2\,i$ meet the conditions of the W-shaped solitons. Interestingly, instead of a higher-order W-shaped soliton, these two localized waves form an oscillation W-shaped soliton with higher intensity ($|A(0,0)|^2 = 4\,(1 + n_1 + n_2)^2$). $|A|^2 \to a^2$ by assuming $z \to \infty$, $t \to \infty$ which gives the asymptotic plane. Due to the nonpropagating characteristic of the nonlinear waves, the nonlinear superposition could show some novel features. The interaction between two same type waves generates a different one.

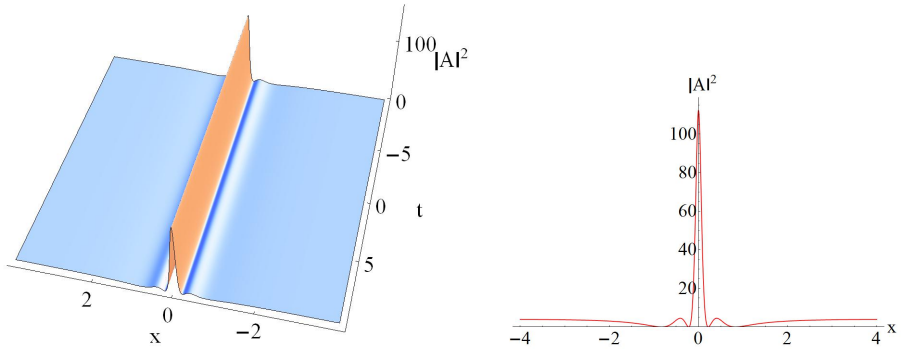

(a) (b)

Figure 10: The interaction between two W-shaped solitons with $a = 2$, $b = 1$, $\gamma = 4$, $\omega = 1$, $\alpha = -1$, $\beta = 1$, $k_1 = 1$, $k_2 = 1$, $\lambda_1 = \lambda_2^* = -0.5 + 2.1\,i$ and $\lambda_3 = \lambda_4^* = -0.5 + 2.2\,i$. The nonlinear interaction forms an oscillation W-shaped soliton.

The W-shaped soliton. Next, we demonstrate the nonlinear interaction between two antidark solitons in **Fig. 11**. The two eigenvalues $\lambda_1 = m_1 + i\,n_1$ and $\lambda_3 == m_3 + i\,n_3$ are set to be $-0.5 - 2.2\,i$ and $-0.5 - 2.3\,i$, respectively. Surprisingly, we find that the interaction between the antidark solitons doesn't produce a second-order antidark soliton, but instead generates a W-shaped soliton.

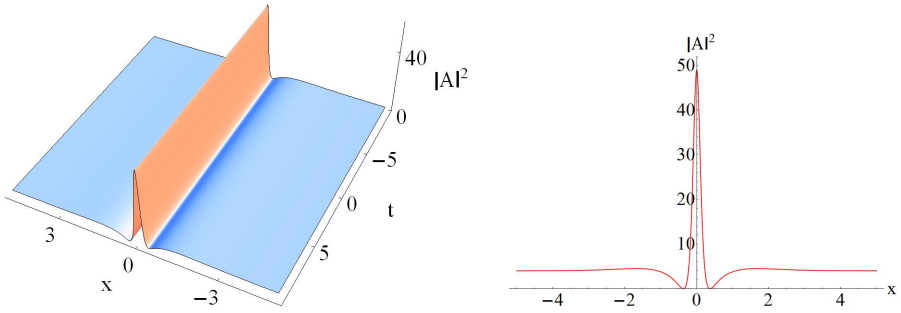

(a) (b)

Figure 11: The interaction between two antidark solitons with $a = 2$, $b = 1$, $\gamma = 4$, $\omega = 1$, $\alpha = -1$, $\beta = 1$, $k_1 = 1$, $k_2 = 1$, $\lambda_1 = \lambda_2^* = -0.5 - 2.2\,i$ and $\lambda_3 = \lambda_4^* = -0.5 - 2.3\,i$. The nonlinear interaction forms a W-shaped soliton.

The antidark soliton and W-shaped soliton pair. We then study the interaction between two different types of nonlinear waves, for example, the antidark soliton and a W-shaped soliton. The eigenvalue $\lambda_1 = -0.5 - 2.1\,i$ is for the antidark soliton while $\lambda_3 = -0.5 + 4\,i$ for the W-shaped one. As shown in **Fig. 12**, an intriguing phenomenon is that the interaction forms an antidark soliton. By adjusting the values of eigenvalues λ_1 (still for antidark soliton) and λ_3 (still for W-shaped soliton), we observe a W-shaped soliton pair in **Fig. 13**. Each component

in the W-shaped soliton pair has the same intensity. In spite of the similar single wave as the seeds, the nonlinear interactions can produce different patterns due to the choices of different eigenvalues λ_1 and λ_3. This means the mechanism of nonlinear superposition is controlled by the two eigenvalues. A complete and analytical study of the control mechanism of such composite solutions is an issue that requires special investigation.

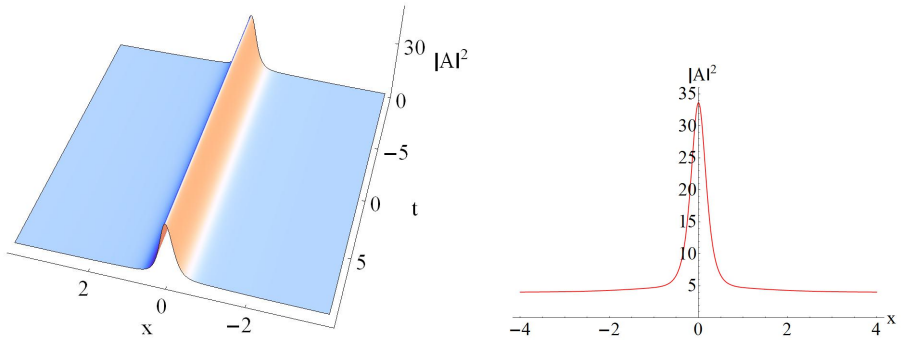

(a) (b)

Figure 12: The interaction between an antidark soliton and a W-shaped soliton with $a = 2$, $b = 1$, $\gamma = 4$, $\omega = 1$, $\alpha = -1$, $\beta = 1$, $k_1 = 1$, $k_2 = 1$, $\lambda_1 = \lambda_2^* = -0.5 - 2.1\,i$ and $\lambda_3 = \lambda_4^* = -0.5 + 4\,i$.

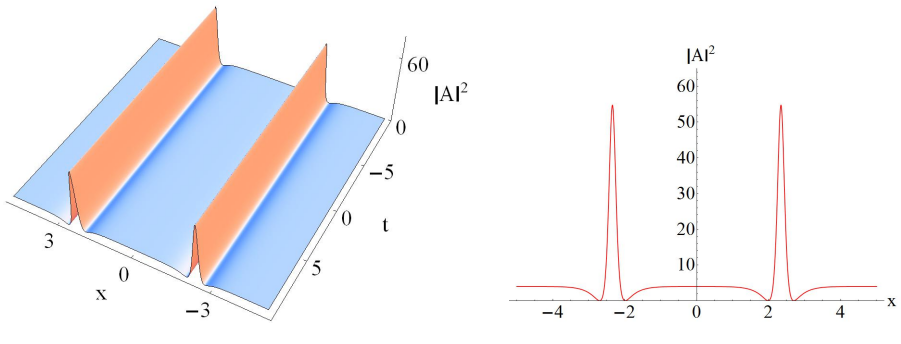

(a) (b)

Figure 13: The interaction between an antidark soliton and a W-shaped soliton with $a = 2$, $b = 1$, $\gamma = 4$, $\omega = 1$, $\alpha = -1$, $\beta = 1$, $k_1 = 1$, $k_2 = 1$, $\lambda_1 = \lambda_2^* = -0.5 - 2.7\,i$ and $\lambda_3 = \lambda_4^* = -0.5 + 2.699\,i$.

The multi-peak solitions. Finally, we display some multi-peak structures. **Fig. 14** describes the nonlinear interactions between the oscillation W-shaped soliton and oscillation M-shaped soliton. The superposition leads to the formation of a three-peak soliton that corresponds to the case $|A(0,0)|^2_{xx} > 0$. Using different eigenvalues, we plot a four-peak soliton ($|A(0,0)|^2_{xx} < 0$) also produced by the oscillation W-shaped soliton and oscillation M-shaped soliton, as depicted in **Fig. 15**. A higher-order multi-peak soiton, which is composed of two first-order multi-peak solitons, is plotted in **Fig. 16**.

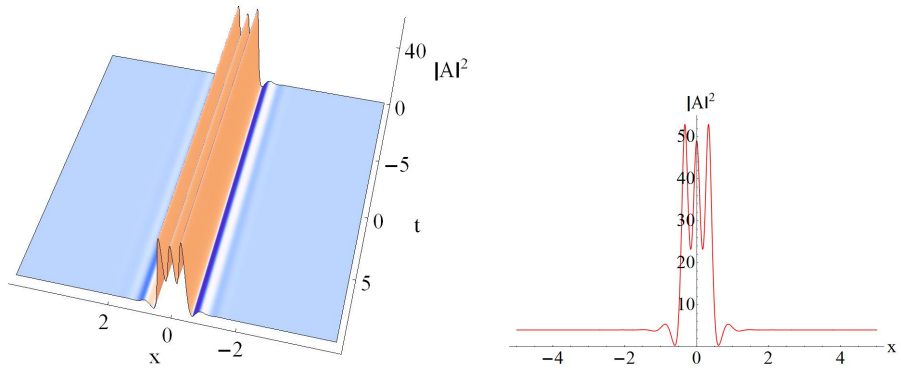

(a) (b)

Figure 14: The interaction between an oscillation W-shaped soliton and an oscillation M-shaped soliton with $a = 2$, $b = 1$, $\gamma = 4$, $\omega = 1$, $\alpha = -1$, $\beta = 1$, $k_1 = 1$, $k_2 = 1$, $\lambda_1 = \lambda_2^* = 4.5 - 2.7\,i$ and $\lambda_3 = \lambda_4^* = 5.5 + 5.2\,i$.

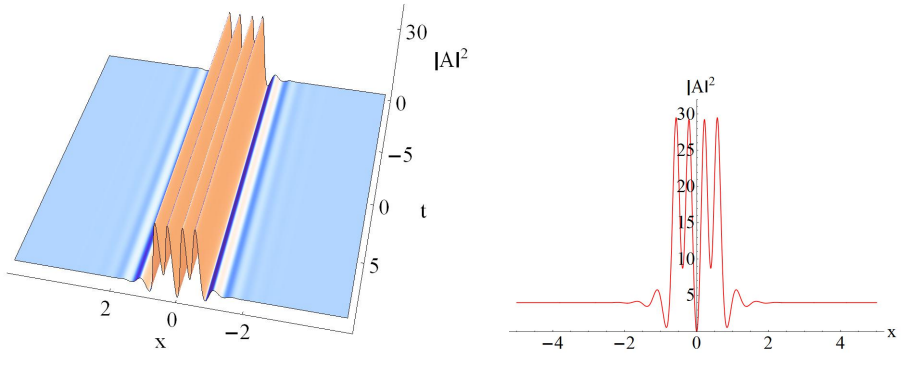

(a) (b)

Figure 15: The interaction between an oscillation W-shaped soliton and an oscillation M-shaped soliton with $a = 2$, $b = 1$, $\gamma = 4$, $\omega = 1$, $\alpha = -1$, $\beta = 1$, $k_1 = 1$, $k_2 = 1$, $\lambda_1 = \lambda_2^* = 6 - 3.05\,i$ and $\lambda_3 = \lambda_4^* = 5 + 2\,i$.

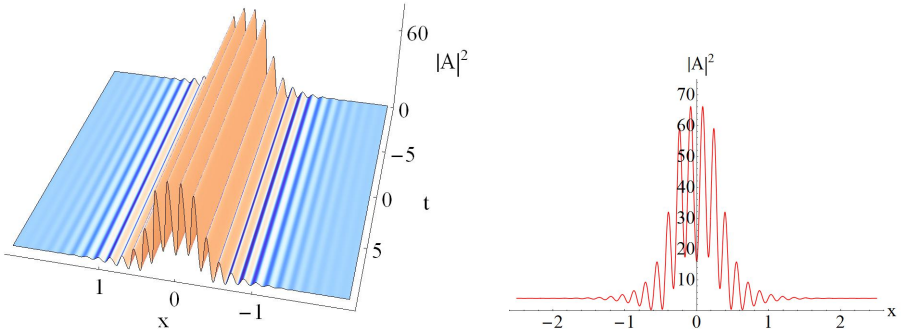

(a) (b)

Figure 16: The interaction between two multi-peak solitons with $a = 2$, $b = 1$, $\gamma = 4$, $\omega = 1$, $\alpha = -1$, $\beta = 1$, $k_1 = 1$, $k_2 = 1$, $\lambda_1 = \lambda_2^* = -19 - 5\,i$ and $\lambda_3 = \lambda_4^* = -20 + 2\,i$.

4. MI characteristics

In this section, we reveal the explicit relation between the transition and the distribution characteristics of MI growth rate for System (2). Firstly, let us recall the results of MI analysis on System (2). As shown in Ref. [18], System (2) admits the following continuous wave solutions,

$$\begin{aligned} A(x,t) &= a\, e^{i\,(\omega\, x + k\, t)}\,, \\ B(x,t) &= b\,, \end{aligned} \tag{16}$$

where a, ω, k and b are real parameters. A perturbed nonlinear background can be expressed as

$$\begin{aligned} A(x,t) &= (a + \epsilon\, \widehat{A}(x,t))\, e^{i\,(\omega\, x + k\, t)}, \\ B(x,t) &= b + \epsilon\, \widehat{B}(x,t). \end{aligned} \tag{17}$$

Taking Eq. (17) into System (2) yields the evolution equation for the perturbations as

$$\begin{aligned} &- a\,\beta\, \widehat{B}(x,t) + i\, k\, \widehat{A}^{(1,0)}(x,t) + i\,\omega\, \widehat{A}^{(0,1)}(x,t) + \widehat{A}^{(1,1)}(x,t) = 0, \\ &\widehat{B}^{(1,0)}(x,t) + \frac{1}{2}\, a\,\gamma\, \widehat{A}^{(0,1)}(x,t) + \frac{1}{2}\, a\,\gamma\, \widehat{A}^{*(0,1)}(x,t) = 0. \end{aligned} \tag{18}$$

Noting the linearity of Eq. (18) with respect to $\widehat{A}$ and $\widehat{B}$, we introduce

$$\begin{aligned} \widehat{A}(x,t) &= U\, \cos(\Lambda\, x - \Omega\, t) + i\, V\, \sin(\Lambda\, x - \Omega\, t)\,, \\ \widehat{B}(x,t) &= K\, \cos(\Lambda\, x - \Omega\, t)\,, \end{aligned} \tag{19}$$

which is characterized by the wave number Λ and frequency Ω. Using Eq. (19) into Eq. (18) gives a linear homogeneous system of equations for U and K:

$$-i\, a\, U\, \Lambda\, k + i\, a\,\omega\, U\, \Omega + i\, a\, V\, \Lambda\, \Omega = 0, \tag{20}$$

$$-a\, V\, \Lambda\, k + a\,\omega\, V\, \Omega - \frac{a^2\, U\,\beta\,\gamma\,\Omega}{\Lambda} + a\, U\, \Lambda\, \Omega = 0. \tag{21}$$

From the determinant of the coefficient matrix of Eqs. (20)$\sim$(21), the dispersion relation for the linearized disturbance can be determined as

$$\Omega^2 \left(-a\beta\gamma + \Lambda^2 - \omega^2\right) - k^2\Lambda^2 + 2k\Lambda\omega\Omega = 0. \tag{22}$$

Solving the above equation, we have

$$\Omega = \frac{k\Lambda\omega \pm \sqrt{k^2\Lambda^2\left(\Lambda^2 - a\beta\gamma\right)}}{a\beta\gamma - \Lambda^2 + \omega^2}. \tag{23}$$

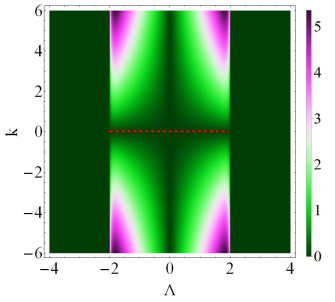

Figure 17: Characteristics of MI growth rate Ω on (Λ, k) plane with $a = 1$, $\gamma = 4$, $\beta = 1$ and $\omega = 1$. Here the dashed red lines represent the stability region in the perturbation frequency region $-a\sqrt{\beta\gamma} < \Lambda < a\sqrt{\beta\gamma}$, which is given as $b = -\frac{\alpha}{\beta}$.

Fig. 17 shows the characteristics of MI on the (Λ, k) plane. It is found that the MI exists in the region $-a\sqrt{\beta\gamma} < \Lambda < a\sqrt{\beta\gamma}$. Ref. [18] has found that the rogue wave existence condition of System (2) is strictly related to baseband MI, namely, the MI whose bandwidth includes arbitrary small frequencies. In this case, we obtain the parameter condition $\beta\gamma > 0$ [18]. Hereby, we discover that the MI growth rate distribution is symmetric with respect to

$$k = 0\,, \tag{24}$$

i.e.,

$$b = -\frac{\alpha}{\beta}. \tag{25}$$

The $k = 0$ line (red dashed line) in Fig. 17 corresponds to a modulational stability (MS) region where the growth rate is vanishing in the low perturbation frequency region. More interestingly, one can find that the MS condition (24) [or (25)] is completely consistent with the condition (7) which converts breathers into stationary nonlinear waves. Our finding suggests that the transition between breathers and stationary nonlinear waves can occur in the MS region with the low frequency perturbations.

5. Conclusions

In summary, we have investigated the transition between breathers and stationary nonlinear waves for System (2). Some intriguing different types of stationary nonlinear waves, including multi-peak solitons, M-shaped soliton, periodic wave, antidark soliton and W-shaped soliton, have been demonstrated graphically and analytically. The reasons and the conditions for transition have been presented explicitly. We have found that the real part of eigenvalue m has effects on the peak numbers of the multi-peak solitons while the imaginary part n controls the transition between the oscillating W-shaped soliton and M-shaped soliton. Further, we have studied the interactions between those transformed nonlinear waves. Due to the nonpropagating characteristic, the nonlinear superposition of two types of nonlinear waves have exhibited some

novel features (see Figs. 10∼16). Finally, we have shown that this transition is strictly associated with the MI analysis that involves a MS region.

Acknowledgements

We express our sincere thanks to all the members of our discussion group for their valuable comments. This work has been supported by the National Natural Science Foundation of China under Grant (Nos. 11305060 and 61505054), by the Fundamental Research Funds of the Central Universities (Project No. 2015ZD16), by the Innovative Talents Scheme of North China Electric Power University, and by the higher-level item cultivation project of Beijing Wuzi University (No. GJB20141001).

References

[1] A. Chabchoub, N. P. Hoffmann, and N. Akhmediev, Phys. Rev. Lett. **106**, 204502 (2011); A. Chabchoub, N. Hoffmann, M. Onorato, and N. Akhmediev, Phys. Rev. X **2**, 011015 (2012).

[2] M. Shats, H. Punzmann, and H. Xia, Phys. Rev. Lett. **104**, 104503 (2010); H. Xia, T. Maimbourg, H. Punzmann, and M. Shats, Rhys. Rev. Lett. **109**, 114502 (2012).

[3] H. Bailung, S. K. Sharma, and Y. Nakamura, Phys. Rev. Lett. **107**, 255005 (2011).

[4] B. Kibler, J. Fatome, C. Finot, G. Millot, F. Dias, G. Genty, N. Akhmediev, and J. M. Dudley, Nat. Phys. **6**, 790 (2010).

[5] Yu. V. Bludov, V. V. Konotop, and N. Akhmediev, Phys. Rev. A **80**, 033610 (2009).

[6] S. Perkins, Sci. News **170**, 328 (2006); E. Pelinovsky and C. Kharif, Extreme Ocean Waves (Springer, Berlin, 2008).

[7] N. Akhmediev, A. Ankiewicz, and M. Taki, Phys. Lett. A **373**, 675 (2009); N. Akhmediev, A. Ankiewicz, and J. M. SotoCrespo, Phys. Rev. E **80**, 026601 (2009); C. Kharif, E. Pelinovsky, and A. Slunyaev, Rogue Waves in the Ocean (Springer, Berlin, 2009); M. Onorato, S. Residori, U. Bortolozzo, A. Montina, and F. T. Arecchi, Phys. Rep. **528**, 47 (2013).

[8] A. D. D. Craik, Wave Interactions and Fluid Flows (Cambridge University Press, 1985). Y. S. Kivshar and G. P. Agrawal, Optical Solitons: From Fibers to Photonic Crystals (Academic Press, 2003).

[9] D. H. Peregrine, J. Aust. Math. Soc. Series B. Appl. Math. **25**, 16 (1983).

[10] V. I. Shrira and V. V. Geogjaev, J. Eng. Math. **67**, 11 (2010).

[11] V. B. Efimov, A. N. Ganshin, G. V. Kolmakov, P. V. E. McClintock, and L. P. Mezhov-Deglin, Eur. Phys. J. Spec. Top. **185**, 181 (2010). M. Shats, H. Punzmann, and H. Xia, Phys. Rev. Lett. **104**, 104503 (2010); A. R. Osborne, Nonlinear Ocean Waves and the Inverse Scattering Transform (Elsevier, Amsterdam, 2010); E. Pelinovsky and C. Kharif, Extreme Ocean Waves (Springer, Berlin, 2008); V. V. Voronovich, V. I. Shrira, and G. Thomas, J. Fluid Mech. **604**, 263 (2008); A. Chabchoub, N. P. Hoffmann, and N. Akhmediev, Phys. Rev. Lett. **106**, 204502 (2011).

[12] D. J. Kedziora, A. Ankiewicz, and N. Akhmediev, Phys. Rev. E **85**, 066601 (2012).

[13] Y. C. Ma, Stud. Appl. Math. **60**, 43 (1979).

[14] N. N. Akhmediev and V. I. Korneev, Theor. Math. Phys. **69**, 1089 (1986).

[15] V. E. Zakharov and L. A. Ostrovsky, Physica D **238**, 540 (2009).

[16] M. S. Ruderman, Eur. Phys. J. Spec. Top. **185**, 57 (2010); A. Slunyaev, Eur. Phys. J. Spec. Top. **185**, 67 (2010); C. Kharif and J. Touboul, Eur. Phys. J. Spec. Top. **185**, 159 (2010).

[17] S. H. Chen, F. Baronio, J. M. Soto-Crespo, P. Grelu, M. Conforti, and S. Wabnitz, Phys. Rev. A **92**, 033824 (2015); F. Baronio, S. H. Chen, P. Grelu, S. Wabnitz, and M. Conforti, Phys. Rev. A **91**, 033804 (2014).

[18] L. Wang, Z. Z. Wang, D. Y. Jiang, F. H. Qi, and R. Guo, Eur. Phys. J. Plus **130**, 199 (2015).

[19] Y. S. Zhang, C. Z. Li, and J. S. He, arXiv: 1505. 02237 (2015).

[20] A. Chowdury, D. J. Kedziora, A. Ankiewicz, and N. Akhmediev, Phys. Rev. E **91**, 032928 (2015).

[21] A. Chowdury, A. Ankiewicz, and N. Akhmediev, Proc. R. Soc. A **471** 20150130 (2015).

[22] J. S. He, S. W. Xu, M. S. Ruderman, and R. Erdélyi, Chin. Phys. Lett. **31**, 010502 (2014).

[23] Y. Ren, Z. Y. Yang, C. Liu, and W. L. Yang, Phys. Lett. A **379**, 2991 (2015).

[24] C. Liu, Z. Y. Yang, L. C. Zhao, and W. L. Yang, Phys. Rev. E **91**, 022904 (2015); C. Liu, Z. Y. Yang, L. C. Zhao, and W. L. Yang, Ann. Phys. **362**, 130 (2015).

[25] Dodd, R. K., Eilkck, J. C., Gibbon, J. D., Moms, H. C.: Solitons and Nonlinear Wave Equations. Academic Press, New York (1982).

[26] A. M. Kamchatnov and M. V. Pavlov, J. Phys. A: Math. Gen. **29**, 3279 (1995).

[27] C. F. Wu, R. H. J. Grimshaw and K. W. Chow, Chaos **25**, 103113 (2015).

[28] R. Guo, H. Q. Hao, and L. L. Zhang, Nonlinear Dynam. **74**, 701 (2013).

[29] B. Tan and J. P. Boyd, Stud. Appl. Math. **109**, 67 (2002).

[30] X. Wang, Y. Q. Li, F. Huang, and Y. Chen, Commun. Nonlinear Sci. Numer. Simulat. **20**, 434 (2015).

[31] Yu. S. Kivshar, Phys. Rev. A **43**, 1677 (1991); Y. S. Kivshar and V. V. Afanasjev, Phys. Rev. A **44**, R1446(R) (1991).